Prediction of crack induced failure phenomena in rolling operations

Available online at www.sciencedirect.com

ScienceDirect

Procedia Manufacturing 15 (2018) 176–184

Procedia MANUFACTURING

www.elsevier.com/locate/procedia

17th International Conference on Metal Forming, Metal Forming 2018, 16-19 September 2018, Toyohashi, Japan

Prediction of crack induced failure phenomena in rolling operations

T. Komischke[a,*], P. Hora[a], G. Domani[b], M. Plamondon[c], R. Kaufmann[c]

[a]*Institute of Virtual Manufacturing, ETH Zurich, 8092 Zurich, Switzerland*
[b]*Hilti AG, 9494 Schaan ,Liechtenstein*
[c]*Swiss Federal Laboratories for Material Science and Technology (EMPA), 8600 Duebendorf, Switzerland*

Abstract

Modern ductile bulk fracture criteria are calibrated and evaluated in cold cross rolling processes using a boron-alloyed tempered steel as a workpiece material. Notches were rolled into more than 400 workpieces in order to investigate the occurrence of core cracks (Mannesmann-effect). The used tools have been designed and produced to deform the workpiece under different stress-triaxialities (0.2 to 0.6) and Lode-Parameters (-0.9 to 0). Both the roller width and the number of workpiece rotations per diameter reduction have been found to be important parameters influencing ductility decisively. The simulative results show a significant influence of both stress-triaxiality and Lode-Parameter on ductility.

Peer-review under responsibility of the scientific committee of the 17th International Conference on Metal Forming.

Keywords: Ductile fracture; Core crack; Mannesmann effect; rolling; Stress triaxiality; Lode parameter; Fracture strain

1. Introduction

Ductile fracture criteria for bulk forming applications are still being investigated extensively. In this paper different criteria will be calibrated by tension and torsion experiments in order to accurately predict fracture strains in cross rolling experiments. It is found that cross rolling experiments can reveal valuable insight into ductile fracture criteria because they deform the workpiece under a variety of Lode-parameters and stress triaxialities. This helps evaluate the performance of different fracture criteria outside of the range of standard experiments used for the criteria's calibration. It can be found that some criteria predict ductility in cross rolling experiments only poorly although they fit standard tension and torsion experiments really well. Other criteria perform significantly better.

* Corresponding author. Tel.: +41446330531.
E-mail address: komischke@ivp.mavt.ethz.ch

2351-9789
Peer-review under responsibility of the scientific committee of the 17th International Conference on Metal Forming.
10.1016/j.promfg.2018.07.192

Nomenclature

ε_f	fracture strain	T	temperature
η	stress triaxiality	$\dot{\varepsilon}$	strain rate
$\bar{\theta}$	normalized Lode angle parameter	JC	Johnson-Cook fracture criterion
ΔD	workpiece diameter reduction	MC	Mohr-Coulomb fracture criterion
U	workpiece rotations	HC	Hosford-Coulomb fracture criterion

1.1. Formulation of fracture criteria

Most ductile fracture criteria are formulated in terms of the invariants of the stress tensor **σ**. These invariants are defined in equation 1-3, where σ_1, σ_2 and σ_3 denote the tensor's principal stresses:

$$I_1 = p = -\sigma_m = -\frac{1}{3}(\sigma_1 + \sigma_2 + \sigma_3), \tag{1}$$

$$I_2 = q = \sigma_e = \sqrt{\frac{1}{2}[(\sigma_1 - \sigma_2)^2 + (\sigma_2 - \sigma_3)^2 + (\sigma_3 - \sigma_1)^2]}, \tag{2}$$

$$I_3 = r = \left[\frac{27}{2}(\sigma_1 - \sigma_m)(\sigma_2 - \sigma_m)(\sigma_3 - \sigma_m)\right]^{\frac{1}{3}}, \tag{3}$$

$$\eta = \frac{-p}{q} = \frac{\sigma_m}{\sigma_e}, \tag{4}$$

$$\bar{\theta} = 1 - \frac{2}{\pi}\arccos\left(\left(\frac{r}{q}\right)^3\right). \tag{5}$$

It is well known that the stress triaxiality η has a significant influence on fracture strains. The dimensionless hydrostatic pressure, also known as stress triaxiality η is given in Eq. (4). The Johnson Cook [1] failure criterion (JC) is a frequently used criterion that relates fracture strain to triaxiality as seen in equation 6. Here it is given without strain rate- and temperature dependence. More recent publications [2-6] show a dependence of ductilitiy also on the Lode parameter. Equation 5 gives the definition of the normalized Lode angle parameter $\bar{\theta}$, used in this article as Lode Parameter. A typical fracture criterion dependent on the Lode parameter is given in [2], see Eq. (7). It extends the JC criterion and assumes a symmetric shape of the boundary surface with respect to $\bar{\theta} = 0$.

$$\varepsilon_f = C_1 + C_2 \exp(-C_3\eta), \tag{6}$$

$$\varepsilon_f = C_1 \exp(-C_2\eta) - (C_1 \exp(-C_2\eta) - C_3 \exp(-C_4\eta))\left(1 - \bar{\theta}^{\frac{1}{n}}\right)^n. \tag{7}$$

Most recent publications indicate that the assumption of symmetry with respect to $\bar{\theta}$=0 seems to be a simplification [3-6]. A typical class of possibly asymmetric fracture criteria are the Mohr-Coulomb (MC) criteria that are extensively used in rock and soil mechanics, but also show good results in predicting ductile fracture [4]. The MC model claims that fracture occurs when the combination of normal stress σ_n and shear stress τ acting at an arbitrary cutting plane defined by normal vector n reaches a critical value. Eqs. (8) and (9) give the MC criterion and are fully equivalent assuming a von Mises yielding function [4]. Eq. (9) can be transformed to the modified Haigh-Westergaard space $\{\eta, \bar{\theta}, \varepsilon_p\}$ through the inverse of the hardening curve. Also [5] concluded from an extensive localization unit cell analysis on a Levy-von Mises material with spherical defects that a Mohr-Coulomb type of model is suitable for predicting the onset of fracture. To improve model accuracy [6] replaced the equivalent Tresca stress in Eq. (8) by the equivalent Hosford stress. Eq. (10) shows the Hosford-Coulomb (HC) criterion. For the transformation of the HC criterion from the principal stress space $\{\sigma_1, \sigma_2, \sigma_3\}$ to the modified Haigh-Westergaard $\{\eta, \bar{\theta}, \varepsilon_p\}$ space the reader is referred to [6].

$$\max_n[\tau + c_1\sigma_n] = c_2\ , \tag{8}$$

$$\sigma_e = c_2 \left[\sqrt{\frac{1+c_1^2}{3}} \cos\left(\frac{\bar{\theta}\pi}{6}\right) + c_1 \left[\eta + \frac{1}{3}\sin\left(\frac{\bar{\theta}\pi}{6}\right)\right] \right]^{-1}, \tag{9}$$

$$\max_{n}[\sigma_{HF} + c_1\sigma_n] = c_2\,, \tag{10}$$

$$\sigma_{HF} = \left[\frac{1}{2}[(\sigma_1 - \sigma_2)^a + (\sigma_2 - \sigma_3)^a + (\sigma_3 - \sigma_1)^a]\right]^{\frac{1}{a}}. \tag{11}$$

2. Material characterization

2.1. Hardening behavior

The hardening behavior of the used boron-alloyed tempered steel has been investigated in dilatometer compression tests. The Hensel- Spittel flow curve's [7] parameters are given in Eq. (12). A good agreement between experimental and simulated force - displacement curves has been observed for tensile and upsetting tests. The good agreement of the fitted curve for large strains has been verified through the comparison of simulated and experimental torque-angle curves in torsion tests. A von-Mises yield locus was used for all simulations. It should be noted that Bauschinger effect is not incorporated in the model although the loading direction is continuously changing throughout the rolling process. This is validated through the good agreement of the measured maximum force and torque values of the rolling processes with the simulated ones (deviation max. 10%).

$$\sigma_y = 880\exp(-0.00125T)\,\varepsilon^{0.1}\dot{\varepsilon}^{0.015}\exp\left(\frac{-0.006}{\varepsilon}\right)[MPa]. \tag{12}$$

2.2. Fracture behaviour

In order to determine the material's ductile fracture behavior torsion tests, torsion tests with superimposed tension, torsion tests with superimposed compression, unnotched round tensile tests and notched round tensile tests have been performed and simulated. Non-constant triaxialities and Lode-Parameters have been averaged through equation 13. The results for all experiments are shown in Table 1.

$$\eta_{av} = \int_0^{\varepsilon_f} \frac{\eta}{\varepsilon_f(\eta,\bar{\theta})}\, d\varepsilon\,. \tag{13}$$

Table 1. Results of tension and torsion experiments.

Nr.	Test type	ε_f	η (Av.)	η (min.), η (max.)	$\bar{\theta}$ (Av.)	$\bar{\theta}$ (min.), $\bar{\theta}$ (max.)	$\dot{\varepsilon}$ (Av.)	T (Av.)
TO1	Torsion+ compression	200%	-0.04	-0.05, -0.03	-0.15	-0.21, -0.08	0.07/s	170 °C
TO2	Pure Torsion	158%	0.0	0.0, 0.0	0	0.0, 0.0	0.1/s	170 °C
TO3	Torsion + tension	140%	0.08	0.08, 0.10	0.21	0.18, 0.24	0.3/s	170 °C
TO4	Torsion + tension	138%	0.16	0.14, 0.2	0.4	0.38, 0.43	0.39/s	170 °C
TE1	Tension, unnotched round bar	80%	0.5	0.33, 0.92	1	1, 1	0.2/s	170 °C
TE2	Tension, notched round bar	73%	0.7	0.47, 0.87	1	1, 1	0.1/s	170 °C
TE3	Tension, notched round bar	56%	0.95	0.56, 1.07	1	1, 1	0.05/s	170 °C

These results seem to be well approximated by all fitted criteria. Fig. 1 shows the fit of the Johnson-Cook (JC), Mohr-Coulomb (MC) and the Hosford-Coulomb (HC) fracture criterion in the modified Haigh-Westergaard space, as well as the data points from table 1 used for calibration (red dots). The MC and HC criteria have been transformed into the modified Haigh-Westergaard space through the inverse of the hardening curve (equation 12) at 170 °C and strain rate 0.1/s. The fitted parameters of the Johnson Cook, Mohr-Coulomb and the Hosford-Coulomb fracture criteria are shown in Table 2. The fit has been performed by minimizing square errors.

Table 2. Coefficients of different fracture criteria.

Johnson Cook (JC)			Mohr-Coulomb (MC)		Hosford-Coulomb (HC)		
C_1	C_2	C_3	C_1	C_2 [MPa]	a	C_1	C_2 [MPa]
0.6060	1.1381	3.9442	0.1608	423.64	1.5232	0.0793	377.58

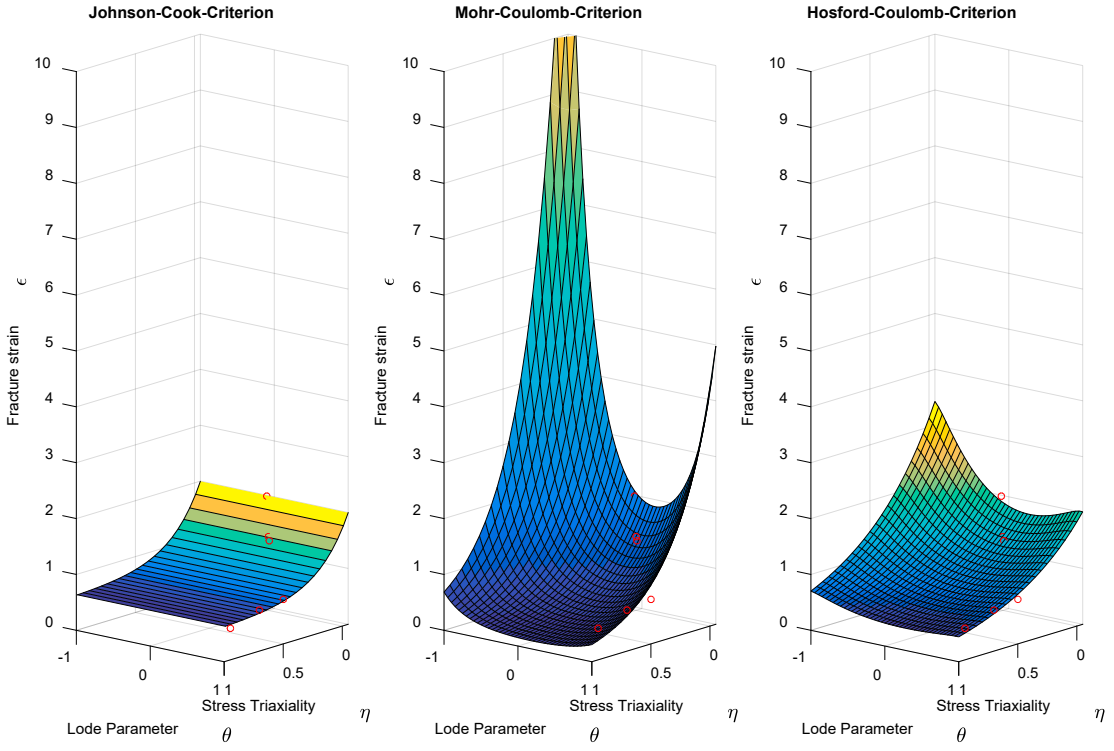

Fig. 1. Fitted fracture criteria in modified Haigh-Westergaard space.

3. Cross rolling experiments

3.1. Experimental setup

Roller segments have been produced with the different widths 5, 7.5, 10, 12.5, 15 and 20 mm (see Fig. 2, right). All Roller segments have an outer diameter of 205 mm. To achieve a sufficient friction coefficient the rollers were sand blasted. Fig. 2 shows the test setup. With these rollers notches have been rolled into steel bars of 10.5 mm diameter. These bars have previously been wiredrawn to obtain straight bars. The bars are held in position by two bushes, one on each side of the roller. Axial elongation is not avoided through the bushes. The rolling process is cooled through an oil-water emulsion.

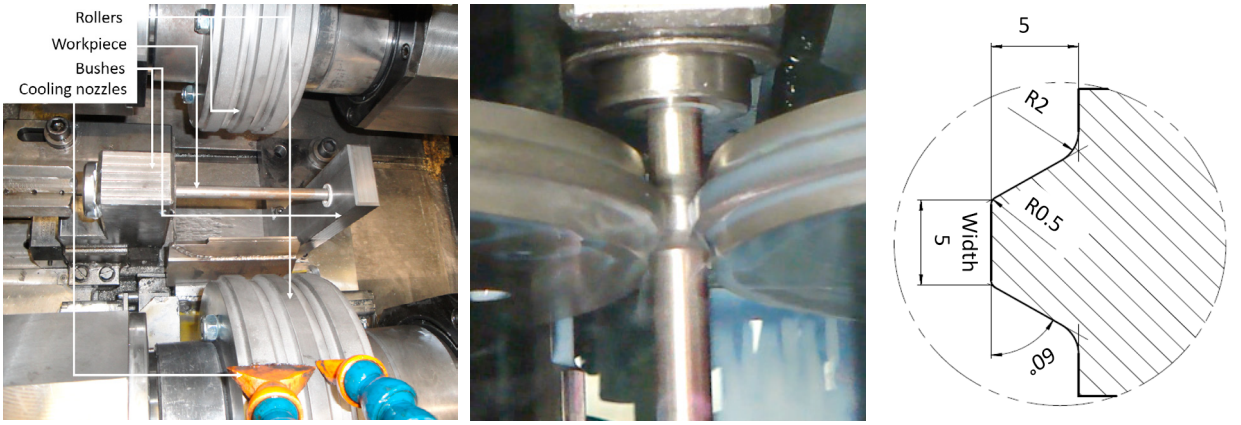

Fig. 2. Cross rolling experiments: Left: Test setup, Middle: Rolling process of notch, Right: Drawing of roller (5mm width).

3.2. Crack investigation

Core crack formation could not be monitored during the forming process, because core cracks cannot be seen from the outside, they are not visible in the measured torque- and force-recordings and an inline failure detection, e.g., using eddy current, was not available . This is why workpieces have been rolled down to different diameters for each of the listed parameter sets (rows in Table 3). These workpieces have later been investigated for internal defects. Comparing the different samples made it possible to determine the diameter at which cracks are observed for the first time, in other words the beginning of the core crack. Most samples have been cut open abrasively, then embedded into a body of synthetic material and then polished down to 5 µm SiC abrasive grains. In order to verify the accuracy of this procedure a total of 30 samples have previously been X-ray investigated. Both 2D and 3D X-ray procedures have been employed. The X-ray resolution was as little as 8 Micrometers. All the cracks that have been seen in the X-ray investigations could also be found after polishing the embedded sample, which validates the applied destructive crack investigation procedure.

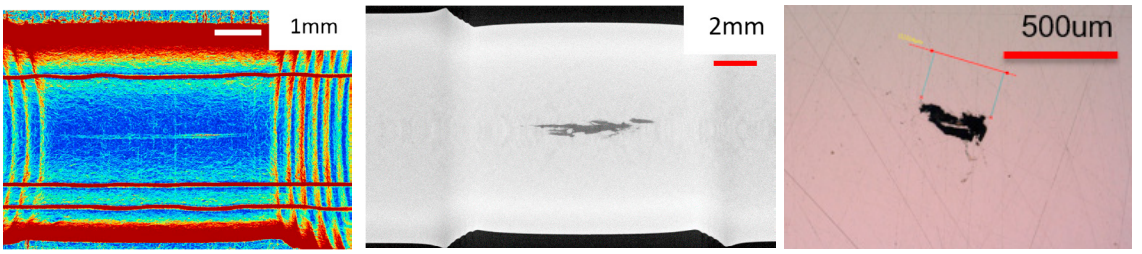

Fig. 3. Crack investigation: Left: 2D X-Ray Scan, Middle: 3D CT Scan, Right: Image of cut and polished sample.

3.3. Experimental design and results

The experimental program given in table 3 has been performed. This program has been derived in a way to cover a wide range of triaxialities and Lode Parameters. For details on how tool design and process parameters affect triaxiality and Lode parameter in the workpiece core see section 4.2. The obtained diameter reductions ΔD at which the crack initiated are also shown in Table 3 for the different process parameters. Note that for each parameter set 5 to 15 different diameter reductions were rolled and for each diameter reduction three to five workpieces were rolled. The given diameter reduction at crack initiation is the average between the lowest diameter reduction for which the majority of the samples were cracked and the highest diameter reduction for which the minority of the samples were cracked. This evaluation procedure reduces deviation of results due to possible variation of material parameters of

single samples. U indicates the number of full workpiece rotations at crack initiation.

Table 3. Cross rolling experimental program and results.

Parameter Set nr.	Roller width	Rotational speed of rollers	U / ΔD	ΔD cracked	ΔD uncracked	ΔD crack initiation	U at crack
R1	20 mm	15 Rpm	6 U/mm	0.35 mm	0.30 mm	*0.325 mm*	2
R2	15 mm	15 Rpm	6 U/mm	0.5 mm	0.40 mm	*0.45 mm*	2.7
R3	10 mm	15 Rpm	6 U/mm	0.92 mm	0.88 mm	*0.9 mm*	5.4
R4	7.5 mm	15 Rpm	6 U/mm	1.7 mm	1.6 mm	*1.65 mm*	9.9
R5	7.5 mm	5 Rpm	2 U/mm	2.25 mm	2.2 mm	*2.225 mm*	4.5
R6	5 mm	10 Rpm	4 U/mm	3.95 mm	3.7 mm	*3.825 mm*	15.3
R7	5 mm	5 Rpm	2 U/mm	5.1 mm	4.7 mm	*4.9 mm*	9.8

4. Simulation of cross rolling processes

4.1. Setup of simulation

A correct process simulation is necessary to obtain reliable results for the strains and stresses until fracture. All simulations have been performed in the commercial Finite element software Simufact with implicit time integration. The workpieces have been meshed with hexahedral elements of an edge size of 0.2 mm in the workpiece core and 0.4 mm otherwise.

The wiredrawing process has been simulated first. Compared to the deformations in the rolling process the deformations of the drawing process are small. Core strains of 10% are reached by drawing, implying a negligible material damage. It was observed that the used rolling machine's spring back cannot be neglected. The overall machine stiffness was determined to be 190 kN/mm. This stiffness is incorporated in the simulation through a spring attached to one of the rollers. The cooling effect of the emulsion had to be quantified as well. To do so, the workpiece temperature has been measured with an infrared camera in the end of the process. Then the process has been simulated. The heat transfer coefficient to the environment has been adapted in the simulation until the temperature at the end of the simulation was equal to the measured one. The heat transfer coefficient has been found to be 25 kW/m^2K. This is a very high value but reasonable due to the evaporating emulsion rinsing the hot workpiece surface. Coulomb friction coefficient has been assumed to be 0.4 due to sand blasted roller surfaces. The workpiece is held in position through spring-loaded sockets. Assumed material properties are given in Table 4.

Table 4. Material parameters used in simulation.

Young's Modulus	Poisson's ratio	Density	Thermal expansion coeff.	Thermal conductivity	Specific heat capacity
210 [GPa]	0.283	7836 [kg/m^3]	1.2*10^-5 [1/K]	47 [W/mK]	490 [J/kgK]

4.2. Simulative results

Fig. 4 shows the equivalent plastic strain and the stress triaxiality for a sectional view of a simulated workpiece at the instant of fracture, rolled with the 10mm roller (parameter set R3) exemplarily. The red dot is radially located in the workpiece core, axially located in the middle of the rolled notch. This is assumed to be the point of crack initiation, as verified by radiographic measurements. All following analyses are performed at this position. Fracture strains and strain evolutions in the workpiece core have been obtained by the numerical simulations introduced in section 4.1. For this reason the correct description of the material's hardening behavior according to chapter 2.1. is of great importance for the results' reliability.

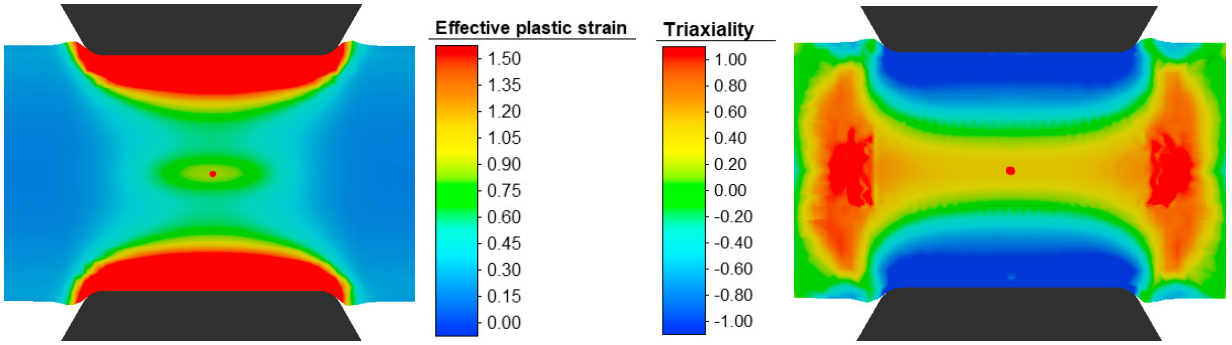

Fig. 4. Left: Plastic strain distribution during rolling process, Right: Triaxiality distribution during rolling process.

The simulation of rolling processes with different roller widths show different triaxialities and Lode Parameters in the workpiece core during forming. Both the simulated triaxiality- and Lode-parameter-paths are shown in Fig. 5 for all parameter sets. The upper row shows the results for a constant rate of 6 workpiece rotations per mm diameter reduction (parameter sets R1, R2, R3, R4) until crack. Wider roller segments cause higher triaxiality and lower norm of the Lode-Parameter. The bottom row in Fig. 5 shows the influence of the rate of workpiece rotations per mm diameter reduction for different roller widths (parameter sets R4, R5, R6, R7). Compare the dashed lines to the solid ones of each color to see that a lower rate of workpiece rotations per diameter reduction reduces stress triaxiality with only minor influence on the Lode-parameter.

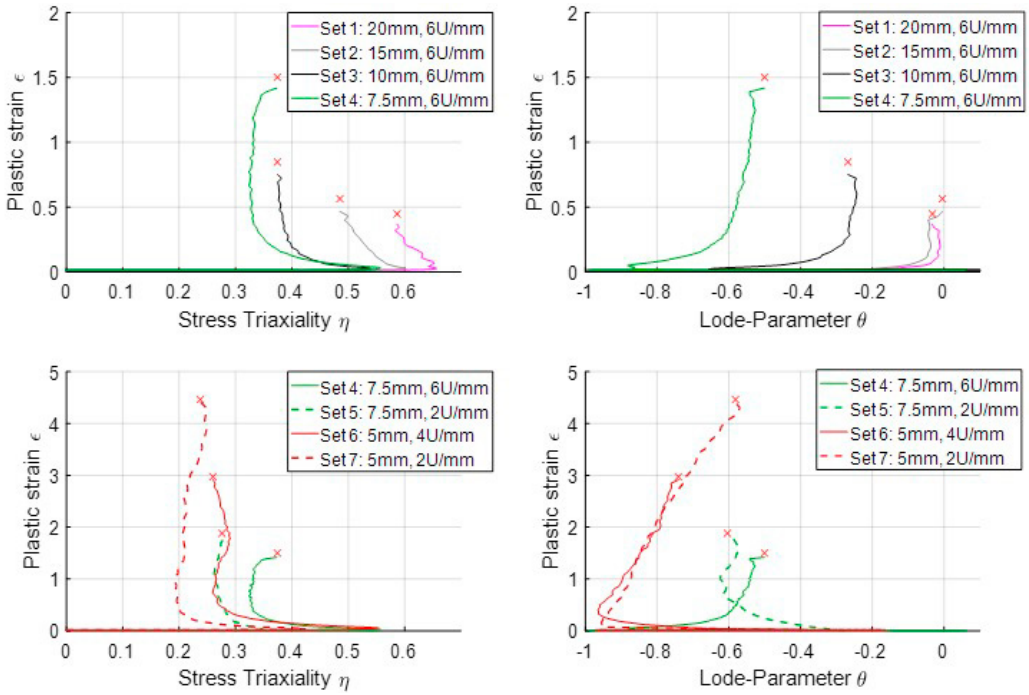

Fig. 5. Triaxiality- and Lode Parameter paths of cross rolling experiments till fracture.

Fig. 6 right summarizes the most important process parameters received through simulation for the different parameter sets. Fig. 6 left shows the core cracks in the space of triaxiality and Lode-Parameter compared to the experimental data from section 2.2. Note that the core cracks happen under triaxiality and Lode-Parameter-combination that have not been investigated in the framework of Lode-parameter dependent ductile fracture criteria yet. They do not happen under plane stress, plain strain or axial symmetry as indicated in Fig. 6 left.

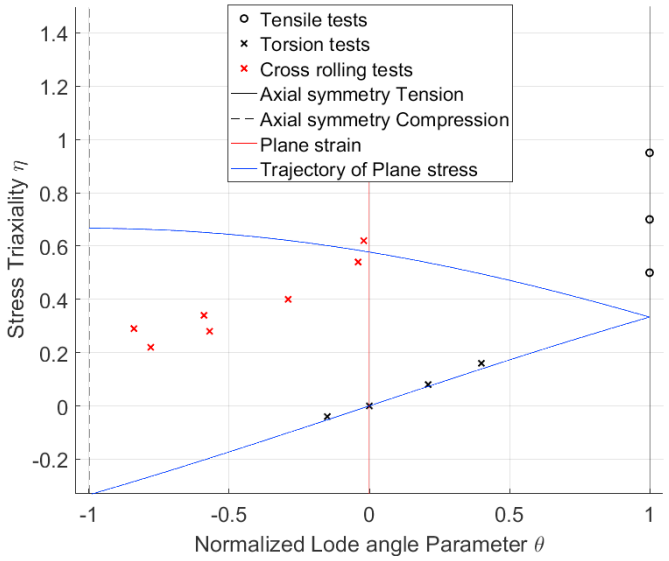

Parameter set Number	ε_f	η (Av.)	$\bar{\theta}$ (Av.)	$\dot{\varepsilon}$ (Av.)	T (max.)
R1	45%	0.62	-0.02	0.80/s	95°C
R2	56%	0.54	-0.04	0.99/s	105°C
R3	85%	0.4	-0.29	0.75/s	200°C
R4	150%	0.34	-0.59	0.68/s	245°C
R5	188%	0.28	-0.57	0.65/s	140°C
R6	297%	0.29	-0.84	0.66/s	195°C
R7	447%	0.22	-0.78	0.57/s	150°C

Fig. 6. Left: All experiments' Lode Parameter and Stress triaxiality, Right: Cross rolling simulative results.

5. Quality assessment of criteria

Table 5 shows the fracture strains predicted by the purely triaxiality dependent JC model and the Lode-dependent asymmetric MC and HC models calibrated only from tension and torsion experiments in section 2.2 and their accuracy. While the JC model meets tension- and torsion experiments very well, relative errors of the JC model are as high as up to 76% for the cross rolling experiments. Note that in the calibration of the JC, HC an MC model it was assumed that ε_f is independent of temperature and strain rate effects, which was in good agreement with experimental data, in particular torsion tests at different temperatures and strain rates. For this reason the representations of the MC and HC criterion in the modified Haigh-Westergaard space $\{\eta, \bar{\theta}, \varepsilon_p\}$ were used and modelled as independent of temperature and strain rate. The HC model predicts fracture strains more precisely than the JC model, while the steep increase of the MC model for low Lode parameter and low triaxiality meets the rolling experiments best with an average relative error of only 14%. It has been shown in [8] that core crack formation in rolling processes can also be due to minor material integrity in the workpiece core. In [8], a workpiece with diameter 200 mm has been used, while this study deals with workpieces of diameter 10.5 mm. This makes the authors assume that the difference in material integrity between core and surface of the rolled bar used in this study is small. For this reason, lower material integrity in the workpiece core is not assumed to falsify results.

Table 5. Quality assessment of different fracture criteria.

Parameter set Number	TO1	TO2	TO3	TO4	TE1	TE2	TE3	R1	R2	R3	R4	R5	R6	R7	Average Error
ε_f	200%	158%	140%	138%	80%	73%	56%	45%	56%	85%	150%	188%	297%	447%	-
JC: Predicted ε_f	194%	174%	144%	132%	76%	68%	63%	70%	74%	84%	90%	98%	96%	108%	-
MC: Predicted ε_f	203%	161%	128%	116%	105%	64%	35%	36%	42%	74%	134%	157%	293%	312%	-
HC: Predicted ε_f	186%	171%	143%	131%	88%	68%	48%	69%	79%	104%	139%	151%	178%	192%	-
JC: Rel. Error in ε_f	*3%*	*10%*	*3%*	*4%*	*5%*	*7%*	*12%*	*56%*	*32%*	*1%*	*40%*	*48%*	*68%*	*76%*	***26%***
MC: Rel. Error in ε_f	*1%*	*2%*	*6%*	*12%*	*31%*	*12%*	*37%*	*20%*	*25%*	*13%*	*11%*	*16%*	*1%*	*30%*	***14%***
HC: Rel. Error in ε_f	*7%*	*8%*	*1%*	*3%*	*10%*	*7%*	*32%*	*35%*	*77%*	*22%*	*7%*	*20%*	*40%*	*57%*	***23%***

6. Conclusion

Rolling operations have been performed with different tools and process parameters leading to core cracks of the workpiece under a wide range of stress triaxialities and Lode- Parameters. The following conclusions can be made:

- The rolling operations lead to core cracks under Lode Parameter-stress triaxiality combinations that are not reached by standard tests. For this reason these tests are revealing from the point of view of ductile fracture research.
- Although the frequently used JC-criterion meets the performed tension and torsion test results very well, it yields much higher errors in rolling experiments due to Lode-Parameters smaller -0.5.
- The findings indicate that there is a strongly Lode dependent, asymmetric fracture surface in the modified Haigh-Westergaard space for the used boron-alloyed tempered steel.
- This surface seems to be well approximated by the simple MC fracture criterion having only two coefficients to be calibrated.

The effect of the cyclic nature of the process on the resulting fracture strains and fracture criteria calibration is part of ongoing research of the authors.

References

[1] G.R. Johnson, W.H. Cook, A constitutive model and data for metals subjected to large strains, high strain rates and high temperatures, Proceedings of the 7th International Symposium on Ballistics, (1983) 541–547.
[2] T. Wierzbicki, Y. Bao, Y.W. Lee, Y. Bai, Calibration and evaluation of seven fracture models, International Journal of Mechanical Sciences, 47-4-5 (2005) 719–743.
[3] Y. Bai, T. Wierzbicki, A new model of metal plasticity and fracture with pressure and Lode dependence, International Journal of Plasticity, 24 (2008) 1071–1096.
[4] Y. Bai, T. Wierzbicki, Application of extended Mohr-Coulomb criterion to ductile fracture, International Journal of Fracture, 161 (2010) 1–20.
[5] M. Dunand, D. Mohr, Effect of Lode parameter on plastic flow localization after proportional loading at low stress triaxialities, Journal of the Mechanicsand Physics of Solids, 66-1 (2014) 133–153.
[6] D. Mohr, S. Marcadet, Micromechanically-motivated phenomenological Hosford-Coulomb model for predicting ductile fracture initiation at low stress triaxialities, International Journal of Solids and Structures, 67-68 (2015) 40–55.
[7] A. Hensel, T. Spittel, Kraft- und arbeitsbedarf bildsamer formgebungsverfahren, Leipzig: Deutscher Verlag für Grundstoffindustrie, (1978).
[8] A. Ghiotti, S. Fanini, S. Bruschi, P.F. Bariani, Modelling of the Mannesmann effect, CIRP Annals- Manufacturing Technology, 58 (2009) 255–258.